British Journal of Pharmacology

DOI:10.1111/bph.13267
www.brjpharmacol.org

RESEARCH PAPER

Molecular dynamics and functional studies define a hot spot of crystal contacts essential for PcTx1 inhibition of acid-sensing ion channel 1a

Natalie J Saez[1†], Evelyne Deplazes[1,2†], Ben Cristofori-Armstrong[1†], Irène R Chassagnon[1], Xiaozhen Lin[#], Mehdi Mobli[3], Alan E Mark[2], Lachlan D Rash[1] and Glenn F King[1,2]

[1]*Institute for Molecular Bioscience, The University of Queensland, St. Lucia, QLD 4072, Australia,* [2]*School of Chemistry and Molecular Biosciences, The University of Queensland, St. Lucia, QLD 4072, Australia, and* [3]*Centre for Advanced Imaging, The University of Queensland, St. Lucia, QLD 4072, Australia*

Correspondence
Professor Glenn F King or Dr Lachlan D Rash, Institute for Molecular Bioscience, The University of Queensland, St. Lucia, QLD 4072, Australia.
E-mail: glenn.king@imb.uq.edu.au; l.rash@uq.edu.au
[#]Present address: Beijing Genomics Institute, Yantian District, Shenzhen, China
[†]These authors contributed equally to this work

Received
29 January 2015
Revised
29 June 2015
Accepted
13 July 2015

BACKGROUND AND PURPOSE

The spider-venom peptide PcTx1 is the most potent and selective inhibitor of acid-sensing ion channel (ASIC) 1a. It has centrally acting analgesic activity and is neuroprotective in rodent models of ischaemic stroke. Understanding the molecular details of the PcTx1 : ASIC1a interaction should facilitate development of therapeutically useful ASIC1a modulators. Previously, we showed that several key pharmacophore residues of PcTx1 reside in a dynamic β-hairpin loop; conclusions confirmed by recent crystal structures of the complex formed between PcTx1 and chicken ASIC1 (cASIC1). Numerous peptide : channel contacts were observed in these crystal structures, but it remains unclear which of these are functionally important.

EXPERIMENTAL APPROACH

We combined molecular dynamics (MD) simulations of the PcTx1 : cASIC1 complex with mutagenesis of PcTx1 and rat ASIC1a.

KEY RESULTS

Crystal structures of the PcTx1 : cASIC1 complex indicated that 15 PcTx1 residues form a total of 57 pairwise intermolecular contacts (<5 Å) with 32 channel residues. MD simulations, however, suggested that about half of these interactions do not persist in solution. Mutation to alanine of only eight of 15 PcTx1 contact residues substantially altered ASIC1a inhibition by PcTx1. Our data reveal that many of the peptide–channel interactions observed in the PcTx1 : cASIC1 crystal structures are not important for PcTx1 inhibition of rat ASIC1a.

CONCLUSIONS AND IMPLICATIONS

We identified the atomic interactions that are critical for PcTx1 inhibition of ASIC1a. Our data highlight the value of combining structural information, MD and functional experiments to obtain detailed insight into the molecular basis of protein : protein interactions.

Non-standard Abbreviations

ASIC, acid-sensing ion channel; βHL, β-hairpin loop; cASIC1, chicken acid-sensing ion channel, isoform 1; ECD, extracellular domain; HMQC, heteronuclear multiple quantum coherence; HSQC, heteronuclear single quantum coherence; MALDI–TOF, matrix-assisted laser desorption/ionization/time-of-flight; MBP, maltose binding protein; MD, molecular dynamics; PcTx1, psalmotoxin 1 (also known as π-theraphotoxin-Pc1a); rASIC1a, rat acid-sensing ion channel, isoform 1a; RP-HPLC, reversed-phase HPLC; TEV, tobacco etch virus; TEVC, two-electrode voltage clamp

Tables of Links

TARGETS	LIGANDS
ASICs	Psalmotoxin 1(PcTx1)

These Tables list key protein targets and ligands in this article which are hyperlinked to corresponding entries in http://www.guidetopharmacology.org, the common portal for data from the IUPHAR/BPS Guide to PHARMACOLOGY (Pawson *et al.*, 2014) and are permanently archived in the Concise Guide to PHARMACOLOGY 2013/14 (Alexander *et al.*, 2013).

Introduction

Acid-sensing ion channels (ASICs) are chordate-specific members of the degenerin/epithelial sodium channel family (Kellenberger and Schild, 2002) that are primarily expressed in the central and peripheral nervous system. They are gated by protons and are the primary acid sensors in mammalian neurons (Waldmann *et al.*, 1997; Gründer and Chen, 2010). ASICs have been implicated in inflammatory and neuropathic pain (Deval *et al.*, 2010; Izumi *et al.*, 2012), psychiatric illnesses (Coryell *et al.*, 2009), seizure termination (Ziemann *et al.*, 2008) and ischaemic stroke (Xiong *et al.*, 2004) and are therefore considered important therapeutic targets (Chu and Xiong, 2013; Wemmie *et al.*, 2013; Dussor, 2015; Li and Xu, 2015).

Six ASIC subunits (ASIC1a/b, ASIC2a/b, ASIC3 and ASIC4) can combine to form homotrimeric or heterotrimeric channels. Each subunit contains a large extracellular domain (ECD), two transmembrane helices and short intracellular N- and C- termini. The subunit composition of each channel determines its pH sensitivity, kinetics and pharmacology (Hesselager *et al.*, 2004; Wemmie *et al.*, 2013). The crystal structure of chicken ASIC1 (cASIC1; orthologue of rodent/human ASIC1a) revealed the trimeric architecture of ASICs and highlighted a negatively charged surface-accessible cavity, termed the 'acidic pocket', at each subunit interface (Jasti *et al.*, 2007). The acidic pocket was proposed to be the main proton-sensing site on ASICs (Jasti *et al.*, 2007), and disruption of carboxyl–carboxylate interactions in this cavity confirmed that this region is central to channel activation (Jasti *et al.*, 2007; Ramaswamy *et al.*, 2013). However, proton gating of ASICs appears to be highly complex as two independent studies also highlighted a role in proton sensing for residues at the top of transmembrane domain 1 in ASIC1a (Paukert *et al.*, 2008) and ASIC2a (Baron *et al.*, 2001).

The most selective and potent inhibitor of ASIC1a reported to date is psalmotoxin 1 (PcTx1), a disulfide-rich peptide isolated from spider venom. PcTx1 inhibits homomeric ASIC1a and heteromeric ASIC1a/2b channels with IC_{50} values of 0.9 and 3 nM, respectively (Escoubas *et al.*, 2000; Sherwood *et al.*, 2011), but it does not inhibit other subtypes (Escoubas *et al.*, 2000; Escoubas *et al.*, 2003). PcTx1 is a gating modifier that stabilizes the desensitized state of ASIC1a (Chen *et al.*, 2005). At higher concentrations, PcTx1 *potentiates* rat and human ASIC1b (Chen *et al.*, 2006; Hoagland *et al.*, 2010) and *opens* cASIC1 (Samways *et al.*, 2009; Baconguis and Gouaux, 2012) by stabilizing the open state of these subtypes.

PcTx1 is a 40-residue peptide stabilized by a classical inhibitor cystine knot motif, with a dynamic β-hairpin loop (βHL) protruding from the disulfide-rich core (Figure 1A) (Escoubas *et al.*, 2003; Saez *et al.*, 2011). Site-directed mutagenesis combined with *in silico* docking revealed that PcTx1 binds into the acidic pocket of ASIC1a, with residues Trp^{24}, Arg^{26} and Arg^{27} within the βHL being critical for PcTx1 inhibition of the channel (Saez *et al.*, 2011). These data supported the results of studies on chimeric ASICs that gave the first indication of regions essential for PcTx1 binding (Chen *et al.*, 2006; Salinas *et al.*, 2006). Two recent crystal structures of the PcTx1 : cASIC1 complex (Baconguis and Gouaux, 2012; Dawson *et al.*, 2012) not only confirmed the importance of the interaction between the βHL and the acidic pocket but also revealed a more extensive network of contacts than would have been predicted from prior functional studies. In both crystal structures, the βHL of PcTx1 is deeply buried in the acidic pocket, making contact with adjacent channel subunits. Additional interactions are made between the thumb domain of one channel subunit and residues in loop 1 and the C-terminal region of PcTx1 (Figure 1B).

The crystal structure of the PcTx1 : cASIC1 complex (PDB 3S3X) reveals an extensive network of 57 intermolecular contacts (which we define as pairwise interactions <5 Å) involving 32 channel and 15 peptide residues (Dawson *et al.*, 2012). However, it has been well documented that only a small subset of 'hot spot' residues typically contributes most of the binding free energy at protein–protein interfaces and that the surface accessibility of a residue correlates poorly with its energetic contribution to a protein–protein interaction (Bogan and Thorn, 1998; Kortemme and Baker, 2002). Thus, we sought to take advantage of the PcTx1 : cASIC1 crystal structure in order to define the subset of PcTx1 residues that are crucial for PcTx1 inhibition of ASIC1a.

In this study, we used molecular dynamic (MD) simulations to predict which PcTx1 residues found at the protein–protein interface in the PcTx1 : cASIC1 crystal structure are likely to be functionally important. We then tested these predictions by performing extensive mutagenesis of PcTx1. We also examined the functional consequence of mutating channel residues in close proximity to bound PcTx1. We show that only a subset of intermolecular contacts observed in the PcTx1 : cASIC1 crystal structure are critical for PcTx1 inhibition of ASIC1a. Identification of these hot spot residues provides a solid platform for rational design of therapeutically useful PcTx1 mimetics.

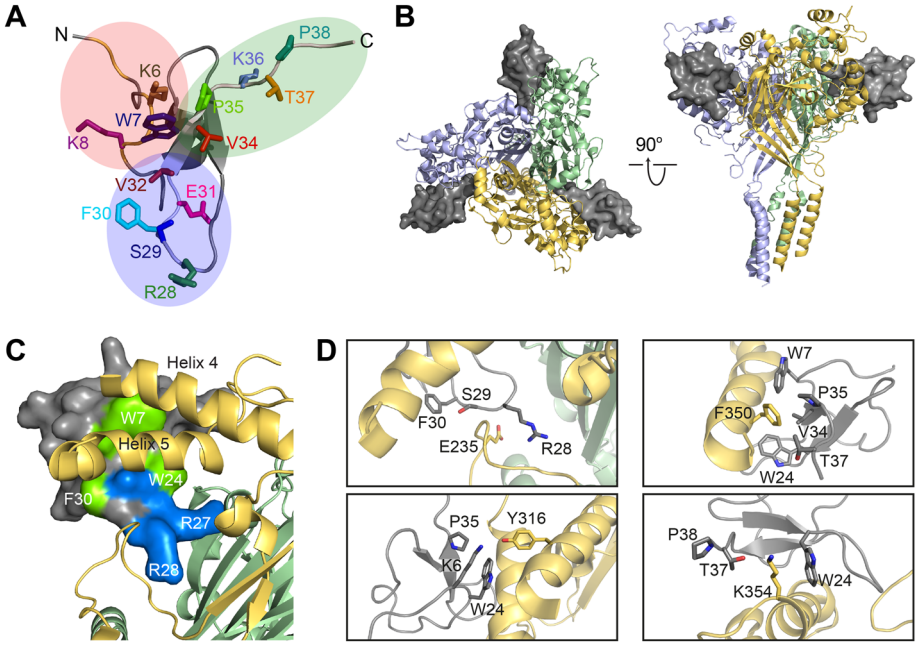

Figure 1

Structure of PcTx1 and its complex with cASIC1. (A) Structure of PcTx1 (PDB 2KNI) highlighting the 13 residues that were mutated to alanine in this study (side chains shown as sticks and labelled). Residues are grouped according to their location in the N-terminal region (red oval), βHL (blue oval) or C-terminal region (green oval). (B) Structure of the PcTx1 : cASIC1 complex (PDB 3S3X). The three cASIC1 subunits are coloured purple, green and yellow, and the three PcTx1 molecules are shown as grey molecular surfaces. Views from the extracellular space (left) and parallel to the membrane (right) show each PcTx1 molecule binding into the acidic pocket between adjacent subunits. (C) Surface representation of PcTx1 binding between subunits viewed from beneath the acidic pocket. The basic residues of the βHL (blue) protrude deep into the acidic pocket, and a hydrophobic patch (green) engages helix 5 of cASIC1. (D) Each box shows an expanded view of channel residues that were mutated in this study and their respective channel contacts predicted from the PcTx1 : cASIC1 complex (PDB 3S3X; side chains shown as sticks and labelled).

Methods

MD simulations

The PcTx1 : cASIC1 crystal structure (PDB 3S3X; Dawson *et al.*, 2012) was used to perform simulations of the ECD of cASIC1 with PcTx1 molecules bound at each of the three subunit interfaces (Figure 1B). The few missing residues in each channel subunit were modelled using the equivalent region from an alternative structure of the PcTx1 : cASIC1 complex (PDB 4FZ0; Baconguis and Gouaux, 2012). The channel protein was truncated at residues Leu^{71} and Val^{427}, and the N- and C- termini were capped with amide and acetyl groups, respectively, to mimic a continuous backbone structure. PropKa (Li *et al.*, 2005) was used to predict the local pKa of all Glu, Asp and His residues. Tautomeric states of His residues were chosen based on the most likely hydrogen-bonding pattern. Disulfide bonds were modelled as in the crystal structure.

All simulations were carried out with GROMACS version 3.3.3 (van der Spoel *et al.*, 2005), using the GROMOS54a7 force field (Schmid *et al.*, 2011). The cASIC1 ECD was solvated with SPC water (Berendsen *et al.*, 1981) and neutralized with 19 Na^+ and 1 Cl^- ion, which corresponds to an overall concentration of 100 mM NaCl. The system was energy minimized, followed by a 2 ns simulation with position restraints on all channel and peptide atoms and a subsequent 2 ns simulation with position restraints on all channel backbone atoms. Simulations (60 ns each) were performed in triplicate using a 2 fs time step. Constant temperature (298 K) was maintained using a Berendsen thermostat (Berendsen *et al.*, 1984) with time constant of 0.1 ps. Isotropic pressure coupling with a time constant of 0.5 ps and a compressibility of 4.5×10^{-5} bar^{-1} was used to maintain pressure at 100 kPa. Non-bonded interactions were calculated using a twin-range method with a 0.8 nm short-range cut-off in which interactions were updated every time step and a long-range cut-off of 1.4 nm in which the van der Waals and electrostatic interactions were updated every 10 steps together with the pairlist. To correct for the effect of truncating the electrostatic interactions beyond the 1.4 nm cut-off, a reaction field correction was applied assuming a dielectric constant of 78. Covalent bonds in the protein and peptide were constrained using LINCS.

Analysis of MD trajectories

Trajectories were analysed using GROMACS analysis tools plus custom tcl and python scripts. Based on a combination of the root mean square deviation of cASIC1 and PcTx1, the potential energy of the system, and the distance between PcTx1 and channel residues as a function of simulation time, the simulations were considered to have equilibrated after ~25 ns. Configurations sampled after 30 ns were used for analysis (600 frames per simulation). In the first phase of analysis, we identified channel residues with any atom

within 5 Å of any side chain atom of PcTx1 contact residues (i.e. Lys^{6}, Trp^{7}, Lys^{8}, Trp^{24}, Lys^{25}, Arg^{26}, Arg^{27}, Arg^{28}, Ser^{29}, Phe^{30}, Val^{32}, Val^{34}, Pro^{35}, Thr^{37} and Pro^{38}). The fractional occurrence of each of these PcTx1 : cASIC1 residue pairs was calculated by counting the number of frames for which residues were within 5 Å for non-bonded interactions and 2.5 Å for hydrogen bonds. Strong hydrogen bonds are typically shorter than 2.2 Å (Jeffrey, 1994; Stone, 1996), but favourable interactions can be present up to 2.5 Å. Electrostatic and hydrophobic interactions are effective over a longer range than hydrogen bonds and can make significant contributions to protein stability and binding energies at distances of 5 Å or longer (Israelachvili and Pashley, 1982; Stone, 1996; Kumar and Nussinov, 2002). We used 5 Å as the cut-off for these interactions to enable direct comparison with contacts previously reported for the PcTx1 : cASIC1 complex (Dawson *et al.*, 2012). The fractional occurrence of each residue pair was averaged over the three peptides in the system and over the three trajectories. A non-bonded interaction was deemed to be persistent if the fractional occurrence was at least 90%; this value was chosen based on a histogram of all fractional occurrences (Supporting Information Figure S4).

Production of recombinant PcTx1 and variants

Recombinant peptides were produced as described previously (Saez *et al.*, 2011; Klint *et al.*, 2013). Briefly, synthetic genes encoding wild-type (WT) or mutant PcTx1, preceded by a tobacco etch virus (TEV) protease cleavage site, were subcloned into a variant of the pLicC-His_6-maltose binding protein (MBP) periplasmic expression vector in which target peptides are expressed as fusions to a His_6-tagged MBP. Fusion proteins were expressed in *Escherichia coli* BL21(λDE3) and isolated from cell lysates using Ni-NTA Superflow resin (Qiagen, Venlo, Netherlands). The His_6-MBP tag was removed from the eluted fusion protein by cleavage with TEV protease, then rPcTx1 was purified using reversed-phase HPLC (RP-HPLC). rPcTx1 contains a non-native N-terminal Ser residue that facilitates TEV cleavage; this recombinant peptide is equipotent with native PcTx1 (Saez *et al.*, 2011).

Purity and integrity of recombinant peptides

Peptide purity was verified using analytical RP-HPLC and MS. Peptides were eluted from an Aquasil C18 column (2.1 × 50 mm Thermo Fisher Scientific, Waltham, MA, USA) connected to a Prominence UPLC system (Shimadzu, Rydalmere, NSW, Australia) using a linear gradient of 10–50% solvent B (90% acetonitrile, 10% H_2O, 0.043% TFA) over 30 min, at a flow rate of 0.25 mL·min^{-1}. Matrix-assisted laser desorption/ionization–time-of-flight (MALDI–TOF) MS was performed using an Applied Biosystems model 4700 Proteomics Bioanalyser (Thermo Fisher Scientific). RP-HPLC fractions of pure peptides were mixed [1:1 (v·v) $^{-1}$] with α-cyano-4-hydroxy-cinnamic acid matrix (7.5 mg·mL^{-1} in 50/50 acetonitrile/H_2O, 0.1% TFA) and MALDI–TOF mass spectra acquired in reflector positive mode. All masses reported are for monoisotopic M + H^+ ions. The folding of rPcTx1 variants was assessed by comparison of their 2D ^{1}H-^{15}N heteronuclear single quantum coherence (HSQC) or heteronuclear multiple quantum coherence (HMQC) NMR spectra with that of WT PcTx1 (Saez *et al.*, 2011). NMR data were acquired as described previously (Klint *et al.*, 2015).

Production of rat ASIC1a mutants

Point mutations were introduced into a rASIC1a-pRK5 plasmid by PCR using standard protocols with Platinum Pfx DNA Polymerase (Thermo Fisher Scientific; Qi and Scholthof, 2008). Mutant cDNA constructs were sequenced to verify incorporation of the desired mutation (Australian Genome Research Facility, Brisbane, Australia).

Electrophysiology

Peptide activity was assessed using two-electrode voltage clamp (TEVC) electrophysiology on *Xenopus laevis* oocytes expressing WT or mutant rASIC1a. Oocyte preparation, cRNA/cDNA injections and electrophysiology were performed as described previously (Saez *et al.*, 2011). We injected 0.25 ng cRNA for WT rASIC1a and 2 ng cDNA for rASIC1a mutants. (In control experiments, the pH-dependent channel properties of rASIC1a were the same regardless of whether we injected cRNA or cDNA.) Currents were elicited by a pH drop from 7.45 to 6.0 every 60 s using a microperfusion system to allow rapid solution exchange (~1.5 mL·min^{-1}) at 21–22°C. Serial dilutions of PcTx1 were administered at pH 7.45 for 55 s between pH stimulations. pH activation curves were determined using a conditioning pH of 7.9 for 55 s (±30 nM PcTx1) before switching to an activating pH of 4.5 to 7.35 for 5 s. Steady-state desensitization (SSD) curves were obtained by exposing oocytes to a conditioning pH ranging from 7.9 to 6.7 for 115 s (±30 nM PcTx1), before pH 5.0 stimulation for 5 s. Currents were normalized to the maximal current evoked in each test condition. In all experiments, the ND96 solution contained 0.1% BSA to minimize adsorption of PcTx1 onto tubing. A nonlinear fit to the data of a four-parameter logistic equation ('sigmoidal dose–response') was used to obtain the half-maximal response (IC_{50} or pH_{50}) and Hill coefficient (n_H). Statistical analyses comparing differences between WT and mutant channels were based on analysis of variance followed by Dunnett's *post hoc* test. Data are mean ± SEM (n = number of oocytes). Oocyte studies complied with the Australian code of practice for care and use of animals for scientific purposes and were approved by The University of Queensland Animal Ethics Committee (Approval No. QBI/059/13/ARC/NHMRC). Oocytes were obtained via recovery surgery performed under tricaine methanesulfonate anaesthesia. The minimum time between surgeries on the same animal was 3 months. All studies involving animals are reported in accordance with the ARRIVE guidelines for reporting experiments involving animals (Kilkenny *et al.*, 2010; McGrath *et al.*, 2010). All drug and molecular target nomenclature used in this report conforms to BJP's Concise Guide to Pharmacology (Alexander *et al.*, 2013).

Results

MD simulations

The fact that a PcTx1 residue is found in close proximity to cASIC1 in a crystal structure of the complex does not necessarily

mean that this pairwise interaction helps stabilize the complex. However, intermolecular contacts that make energetically important contributions to a protein : protein interaction are likely to persist in solution. MD simulations are ideally suited for studying the temporal nature of protein–ligand interactions (Durrant and McCammon, 2011), and therefore, we performed MD simulations of the PcTx1 : cASIC1 complex in solution in order to predict which contacts observed in the crystal structure are likely to be persistent and functionally important. Table 1 reports the percentage of time that each intermolecular interaction persisted in the simulations and highlights hydrogen bonds and non-bonded interactions formed by side chains of PcTx1 residues that are predicted to persist in solution. The MD simulations did not reveal any persistent intermolecular contacts that were not evident in the PcTx1 : cASIC1 crystal structures.

Only 31 of the 57 non-bonded interactions observed in the PcTx1 : cASIC1 crystal structure (Baconguis and Gouaux,

Table 1

Intermolecular interactions observed in the PcTx1 : cASIC1 crystal structure (Baconguis and Gouaux, 2012; Dawson *et al.*, 2012) and their persistence (% occurrence) in triplicate 30 ns MD simulations

PcTx1	Channel chain A	Channel chain B	% 5 Å cut-off	% 2.5 Å cut-off	PcTx1	Channel chain A	Channel chain B	% 5 Å cut-off	% 2.5 Å cut-off
Lys^{6}		Tyr^{317}	13%		**Arg^{27}**	**Phe^{174}**		96%	
		Asn^{321b}		16%		Phe^{175}		85%	
		Glu^{343}	0%			**Arg^{176}**		90%	
Trp^{7}		**Tyr^{317}**	100%			**Gly^{177}**		94%	
		Asn^{321b}		45%		Thr^{215b}			36%
		Glu^{343}	100%			Gly^{216b}			38%
		Cys^{344}	100%			Asn^{217}		83%	
		Pro^{347}	100%			Gly^{218b}			59%
		Ala^{348}	100%			**Glu^{220a,b}**		99%	37%
		Phe^{351}	100%				**Glu^{354}**	99%	
Lys^{8}		**Glu^{343}**	99%				Asp^{408a}	64%	
Trp^{24}	Gly^{177b}			36%	**Arg^{28}**	Gln^{271}		11%	
	Glu^{178}		98%				Glu^{236}	33%	
		Pro^{347}	92%				Thr^{237}	85%	
		Asp^{350a}	100%				**Asp^{238a}**	98%	
		Phe^{351}	100%				**Thr^{240}**	93%	
		Glu^{354}	100%				**Phe^{242}**	90%	
		Lys^{355}	100%				Glu^{243b}		0%
Lys^{25}	Phe^{174}		73%		**Ser^{29}**		Glu^{236b}		0%
	Gly^{177}		18%				Thr^{237}	72%	
	Gln^{179b}			7%			**Asp^{238a}**	93%	
Arg^{26}	Phe^{174}		0%		**Phe^{30}**		Glu^{236}	65%	
		Asp^{238a}	77%				**Lys^{342}**	95%	
		Lys^{342}	91%		**Val^{32}**		**Pro^{347}**	99%	
		Asp^{346a}	100%		**Val^{34}**		**Phe^{351}**	100%	
		Pro^{347}	100%		**Pro^{35}**		Tyr^{317}	12%	
		Asp^{350a}	100%				**Phe^{351}**	96%	
					Thr^{37}		Phe^{351}	44%	
							Lys^{355}	99%	
					Pro^{38}		Lys^{355}	68%	

Cut-offs of 2.5 and 5 Å were used to calculate fractional occurrence for hydrogen bond and other non-bonded interactions respectively. Residues predicted by MD to form persistent interactions in solution are highlighted in bold.

[a]Putative proton sensors.

[b]Residues predicted to form hydrogen bonds.

2012; Dawson *et al.*, 2012) are predicted to persist in solution. No close contacts involving PcTx1 residues Lys^{6} and Lys^{25}, and only one of three contacts observed for Ser^{29}, are predicted to persist in solution. The MD simulations predict that more than half of the persistent PcTx1 interactions (18 of 31) are formed by just four residues (Trp^{24}, Arg^{26}, Arg^{27} and Arg^{28}) in the βHL, consistent with previous functional studies (Saez *et al.*, 2011). The simulations also suggest that Trp7 in loop 1 might be functionally important as it forms stable contacts with six channel residues. None of 10 intermolecular hydrogen bonds identified in the PcTx1 : cASIC1 crystal structure had consistently high fractional occurrences across the three independent simulations (Supporting Information Figure S4).

The first reported structure of cASIC1 (Jasti *et al.*, 2007) revealed three pairs of proximal Asp and Glu residues within the acidic pocket (Asp^{238}–Asp^{350}, Glu^{239}–Asp^{346} and Glu^{220}–Asp^{408}). These carboxyl–carboxylate pairs are key sites for pH-sensing by ASICs (Jasti *et al.*, 2007; Ramaswamy *et al.*, 2013). In our MD simulations, Asp^{238} was found within 5 Å of Arg^{26}, Arg^{28} and Ser^{29} for most of the simulation time (77, 98 and 93%, respectively). Asp^{346} and Asp^{350} were within 5 Å of Arg^{26} for the entire simulation, and Asp^{350} showed persistent contact with Trp^{24}. Finally, Glu^{220} was within 5 Å of Arg^{27} for 99% of the simulation time, and the same PcTx1 residue was within 5 Å of Asp^{408} for 64% of the simulation time. In summary, five out of the six putative proton-sensing residues were within 5 Å of at least one PcTx1 residue for the vast majority of the simulation time.

Functional importance of N-terminal PcTx1 residues

PcTx1 activity was confirmed using TEVC assays on *Xenopus* oocytes expressing rASIC1a. The measured IC_{50} of 0.35 ± 0.04 nM for WT PcTx1 agrees well with previous studies (Escoubas *et al.*, 2000; Saez *et al.*, 2011). To identify PcTx1 residues critical for inhibition of ASIC1a, we tested the ability of 13 alanine mutants (Figure 1) and two truncation mutants to modulate the activity of rASIC1a. Figure 2 shows concentration–effect curves, and Table 2 shows the corresponding IC_{50} (or EC_{50}) values for all 15 PcTx1 variants. Natural abundance 2D ^{1}H-^{15}N HMQC or HSQC spectra acquired of each variant confirmed that most mutations did not perturb the structure of PcTx1.

Deletion of the two N-terminal residues (i.e. Glu^{1} and Asp^{2}; ΔN2) did not alter PcTx1 potency (Figure 2A; Table 2), suggesting that the deleted residues are not functionally important. This is consistent with the absence of channel contacts observed for these residues in the PcTx1 : cASIC1 crystal structure. Mutation of Trp^{7} to Ala had minimal effect on the structure of PcTx1 as assessed by NMR (Supporting Information Figure S1), but it almost abolished PcTx1 activity (Figure 2A, Table 2). This indicates that Trp^{7} is functionally critical, as might be expected from the numerous contacts it makes with residues within helices 4 and 5 of the thumb region of cASIC1 in MD simulations. Mutation of Lys^{6} to Ala caused a 97-fold decrease in PcTx1 activity. However, comparison of 2D HSQC spectra of the K6A mutant and WT PcTx1 (Supporting Information Figure S1) revealed that this mutation causes substantial differences in chemical shifts of the backbone and indole ring signals of Trp^{7}, suggesting that the loss of activity is likely caused by structural differences within or surrounding Trp^{7} rather than loss of channel interactions with Lys^{6}. Mutation of Lys^{8} to Ala caused only a minor decrease in the inhibitory activity of PcTx1, despite the MD studies predicting a close contact between this residue and Glu^{343} in cASIC1 (Table 1).

Functional importance of residues in the PcTx1 βHL

Mutating Glu^{31} to Ala did not significantly affect PcTx1 activity (Figure 2B, Table 2), consistent with the absence of intermolecular contacts for Glu^{31} in the crystal structure. In contrast, the IC_{50} for inhibition of rASIC1a was increased 14.5-fold for the R28A mutant (Figure 2B, Table 2). In contrast with the PcTx1 : cASIC1 structure solved by Dawson *et al.* (2012) (PDB 3S3X), Arg^{28} did not make close contacts with Glu^{236} or Glu^{243} in the MD simulations. Rather, Arg^{28} was close to Phe^{242}, Thr^{240} and the putative proton-sensing residue Asp^{238} (Table 1) as observed in the structure reported by Baconguis and Gouaux (2012) (PDB 4FZ0). Regardless of its exact mode of binding, Arg^{28} clearly makes energetically favourable interactions with the channel. Surprisingly, the F30A mutant potentiated rather than inhibited rASIC1a (EC_{50} ~7 nM; Figure 2B, Table 2). In the MD simulations (Table 1) and both crystal structures, Arg^{26} and Phe^{30} are the only PcTx1 residues within 5 Å of channel residue Lys^{342}. Interestingly, as found for F30A in this study, an R26A mutant potentiates rASIC1a (Saez *et al.*, 2011).

Mutation of Ser^{29} to Ala did not significantly alter PcTx1 activity despite the potential for this residue to interact with channel residue Asp^{238} (Table 1). In the PcTx1 : cASIC1 crystal structure, Val^{32} contacts only one channel residue (Pro^{347}), yet mutation of Val^{32} to Ala caused an 18-fold decrease in PcTx1 activity. This residue is largely buried at the base of the β-hairpin. This raised the question as to whether the reduced activity of the V32A mutant results from loss of important PcTx1 : channel interactions or is due to structural perturbations induced by the mutation. The 2D ^{1}H-^{15}N HSQC spectrum of the V32A mutant reveals that while the chemical shifts for most residues are very similar to those in WT PcTx1 (Supporting Information Figure S2), substantial chemical shift differences were observed for βHL residues that are important for inhibition of ASIC1a, namely Trp^{24}, Arg^{26}, Arg^{27}, Arg^{28} and Phe^{30}. We therefore conclude that the diminution in activity caused by the V32A mutation results from induced structural changes in the βHL.

Functional importance of C-terminal PcTx1 residues

Deletion of the three C-terminal residues (i.e., Pro^{38}, Lys^{39} and Thr^{40}; 1–37, ΔC3) caused a minor fourfold reduction in PcTx1 potency (Figure 2D; Table 2). Mutation of Pro^{38} to Ala also resulted in a fourfold decrease in potency (Figure 2D; Table 2), suggesting that loss of this residue may be entirely responsible for the decreased potency of

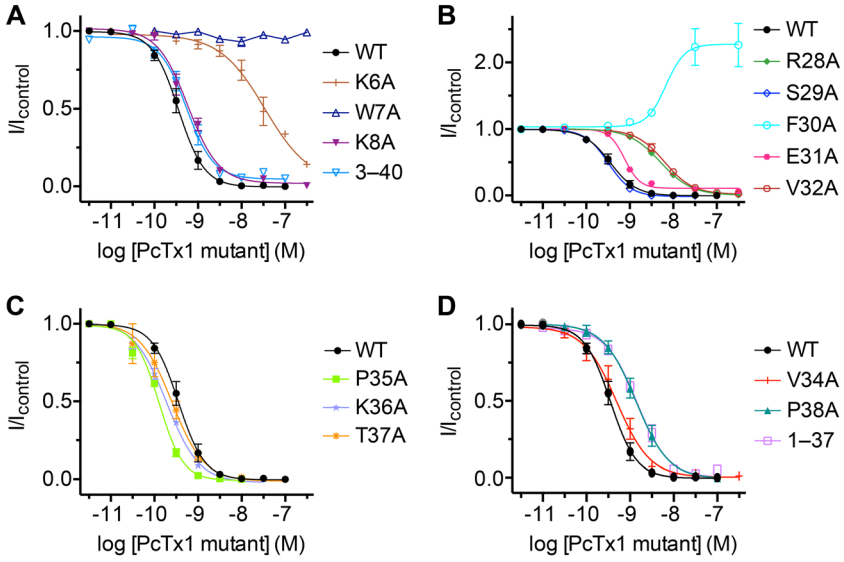

Figure 2

Concentration–effect relationships for modulation of rASIC1a by PcTx1 and various analogues. Data are grouped according to the structural regions highlighted in Figure 1, namely the (A) N-terminus, (B) βHL and (C-D) C-terminus. Data points are mean ± SEM (n = 4–8). The IC_{50} values and Hill coefficients obtained from nonlinear fits of the Hill equation to the concentration–effect data are summarized in Table 2.

Table 2

IC_{50}/EC_{50} values for WT PcTx1 and each of the variants tested (point mutations and truncations)

Peptide	IC_{50} (nM)	Hill slope	Fold change[a]
WT	0.35 ± 0.04	1.5 ± 0.04	—
K6A	34.2 ± 0.23	0.8 ± 0.26	**97.7**
W7A	>1000	N/A	>**2857**
K8A	0.59 ± 0.05	1.2 ± 0.15	1.7
3–40, ΔN2	0.55 ± 0.06	1.4 ± 0.25	1.6
R28A	5.06 ± 0.03	1.2 ± 0.10	**14.5**
S29A	0.32 ± 0.02	1.6 ± 0.12	*1.1*
F30A	6.79 ± 0.30[b]	2.0 ± 0.48	N/A
E31A	0.76 ± 0.02	2.5 ± 0.30	2.2
V32A	6.27 ± 0.04	1.3 ± 0.14	**17.9**
V34A	0.49 ± 0.07	1.1 ± 0.18	1.4
P35A	0.13 ± 0.02	1.6 ± 0.12	*2.7*
K36A	0.19 ± 0.03	1.2 ± 0.09	*1.8*
T37A	0.25 ± 0.06	1.2 ± 0.17	*1.4*
P38A	1.36 ± 0.06	1.2 ± 0.18	3.9
1–37, ΔC3	1.44 ± 0.04	1.2 ± 0.14	4.1

Data are mean ± SEM.
[a]Fold-change in activity relative to WT PcTx1. Italicized numbers indicate an increase in potency. Bold numbers indicate mutants that substantially diminish PcTx1 inhibition of rASIC1a.
[b]Denotes potentiators.

ΔC3. Despite making multiple intermolecular contacts in the PcTx1 : cASIC1 crystal structure and our MD simulations, mutation of none of the other C-terminal residues (V34A, P35A, K36A and T37A) had any appreciable effect on the ability of PcTx1 to inhibit rASIC1a (Figure 2C, D; Table 2).

Assessment of rASIC1a residues predicted to interact with PcTx1

Our MD simulations identified a subset of cASIC1 residues that persistently interact with PcTx1 in solution. To experimentally test the MD predictions, we constructed a panel of rASIC1a mutants (E235A, Y316A, K354A and F350A; E236A, Y317A, K355A and F351A in cASIC1) and examined the effect of WT PcTx1 on each mutant. PcTx1 affects the pH of both activation and SSD of rASIC1a (Chen *et al.*, 2005), and therefore, we determined these parameters for each channel mutant (Supporting Information Figure S3 and Table S1) before examining whether they were altered in the presence of 30 nM WT PcTx1 (Figure 3; Supporting Information Table S1). For the E235A, Y316A and K354A channel mutants, PcTx1 induced a shift in the average pH_{50} of activation and SSD that was comparable to that of WT ASIC1a (Figure 3). Thus, Glu^{235}, Tyr^{316} and Lys^{354} are not critical for PcTx1 modulation of ASIC1a activity. In contrast, PcTx1 had no effect on the pH_{50} of activation or SSD for the F350A mutant (Figure 3; Supporting Information Figure S3), consistent with Phe^{350} being a key residue for interaction with PcTx1. The inhibitory efficiency of 30 nM PcTx1 was similar for all channel mutants (87–98%) when applied at 0.10–0.15 pH units higher than the pH_{50} of SSD with the exception of F350A for which there was no inhibition (Supporting Information Figure S3).

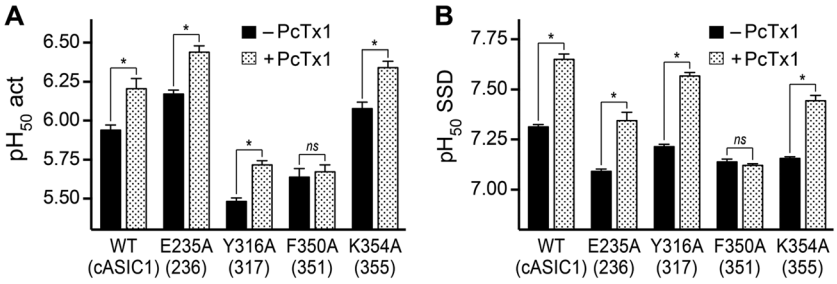

Figure 3

Effect of PcTx1 on pH-dependent properties of native and mutant rASIC1a. Average pH_{50} of (A) activation and (B) SSD in the absence and presence of 30 nM PcTx1. Data are mean ± SEM (n = 4–8). *ns*, not significant, and *$P < 0.005$ (comparison of pH_{50} in the absence and presence of PcTx1). Residues are numbered according to the sequence of rASIC1a, with cASIC1 numbering in parentheses.

Discussion

ASIC1a is a therapeutic target for diverse diseases including chronic pain and stroke. PcTx1 is the most potent and selective inhibitor of ASIC1a reported to date, making it a valuable pharmacological tool and potential therapeutic lead. Crystal structures of the PcTx1 : cASIC1 complex (Baconguis and Gouaux, 2012; Dawson *et al.*, 2012) revealed that the hydrophobic groove at the base of the βHL of PcTx1 interacts with helix 5 of the cASIC1 thumb domain, while the side chains of Arg^{27} and Arg^{28} interact with the negatively charged residues within the acidic pocket, thereby inducing and stabilizing the open state of cASIC1. These structures provide an excellent foundation for understanding the PcTx1 : ASIC1a interaction and developing therapeutically useful PcTx1 mimetics. However, rational design of small-molecule mimetics requires an understanding of which residues at the protein–protein interface make the largest contributions to the free energy of binding. Guided by the PcTx1 : cASIC1 crystal structures, we combined MD simulations with mutagenesis of interface residues to determine which PcTx1 residues are critical for interaction with ASIC1a.

Unrestrained MD simulations revealed that almost half of the interfacial contacts observed in PcTx1 : cASIC1 crystal structures do not persist in solution. Dawson *et al.* (2012) reported 57 interfacial contacts in the PcTx1 : cASIC1 crystal structure contributed by 32 cASIC1 and 15 PcTx1 residues (Dawson *et al.*, 2012). Only 31 of these intermolecular interactions, involving 20 channel and 12 peptide residues, persisted in a significant proportion of the configurations sampled during MD simulations.

We used alanine-scanning mutagenesis to test predictions from the MD simulations and refine the list of critical PcTx1 contact residues. Five of the 13 residues mutated in this study (Lys^6, Trp^7, Arg^{28}, Phe^{30} and Val^{32}) resulted in profound changes in the ability of PcTx1 to inhibit rASIC1a. The W7A mutant was almost completely inactive, while an R28A mutation reduced potency ~15-fold. In both cases, the substantial reduction in activity appears directly related to the loss of key side chain–side chain interactions. Both residues make extensive contacts with multiple channel residues in both the crystal structures and the MD simulations, and NMR data indicate that neither mutation substantially perturbs the structure of PcTx1. In a previous study we demonstrated a similarly profound loss of activity for W24A and R27A mutations, again without concomitant perturbation of the PcTx1 structure (Saez *et al.*, 2011). Thus, we conclude that residues Trp^{24}, Arg^{27} and Arg^{28} in the βHL and Trp7 in loop 1 form the primary hot spot that mediates interaction of PcTx1 with rASIC1a (Figure 4). This is consistent with the observation that Arg and Trp residues are highly enriched in protein–protein interaction epitopes (Bogan and Thorn, 1998).

The effect of mutating Phe^{30} to Ala was unexpected, but similar to what we previously reported for a R26A mutation (Saez *et al.*, 2011). Both mutations result in peptides that potentiate rather than inhibit rASIC1a. The R26A and F30A mutant peptides appear to bind rASIC1a and stabilize the open, rather than the desensitized, state. NMR studies on PcTx1 revealed that the βHL is flexible and that Arg^{26} and Phe^{30} form a cation-π interaction across the base of this loop (Saez *et al.*, 2011). Dawson and colleagues also noted this interaction in the PcTx1 : cASIC1 crystal structure (Dawson *et al.*, 2012). PcTx1 inhibits rat and human ASIC1a by stabilizing the desensitized state of the channel, and this effect appears to be primarily mediated by the side chains of Arg^{27} and Arg^{28} entering the acidic pocket and mimicking the action of protons. It is likely that Arg^{26} and Phe^{30} play a role in stabilizing the βHL of PcTx1 so that the side chains of Arg^{27} and Arg^{28} can be appropriately positioned to interact with carboxyl–carboxylate pairs in the acidic pocket. These residues also make interactions with helix 5 of the channel. Thus, we propose that the dramatic reversal of activity for the R26A and F30A mutants is due to the loss of intermolecular channel interactions combined with altered intramolecular peptide interactions.

The reduced potency of the K6A and V32A peptides is probably due to structural perturbations induced by the mutations. MD simulations suggest that Lys^6 does not form any persistent close contacts with rASIC1a. NMR analysis indicated that the K6A mutation perturbs the conformation of the adjacent and functionally critical Trp^7 (Supporting Information Figure S1), and this is probably the cause of the reduction in activity. However, in the absence of a more conservative mutation, we cannot exclude the possibility that Lys^6 engages in energetically important interactions with rASIC1a.

Mutation of PcTx1 residues predicted not to interact with rASIC1a (Glu^{31} and Lys^{36}) had little to no effect on peptide activity. Mutations of Lys^8 or Pro^{35} were also not deleterious

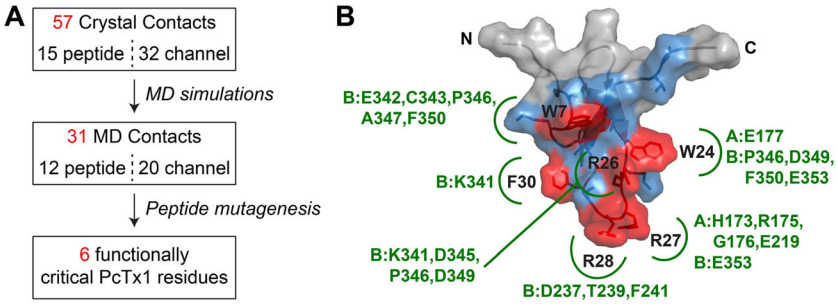

Figure 4

Key intermolecular interactions between PcTx1 and rASIC1a. (A) Flow diagram showing the process by which we identified key contacts for the PcTx1 : rASIC1a interaction. (B) Surface representation of PcTx1 highlighting residues (blue and red) that make intermolecular contacts in crystal structures of the PcTx1 : cASIC1 complex (Baconguis and Gouaux, 2012; Dawson *et al.*, 2012). Alanine-scanning mutagenesis revealed that only the residues shown in red are critical for interaction with rASIC1a. Shown in green are channel residues that, based on channel mutagenesis and MD simulations, appear to make the most energetically important interactions with each of the PcTx1 hot spot residues (rASIC1a numbering, with 'A' and 'B' denoting subunit). The N- and C- termini are labelled.

even though these residues persistently interacted with channel residues Glu^{343} and Phe^{351}, respectively, in MD simulations. Lys^{25} makes several interfacial contacts in one of the PcTx1 : cASIC1 crystal structures (Dawson *et al.*, 2012), but not the other (Baconguis and Gouaux, 2012), and no persistent interactions were observed in the MD simulations. Consistent with these observations, we previously showed that a K25A mutant is equipotent with native PcTx1 (Saez *et al.*, 2011). Thus, Lys^{25} is not functionally important. Ser^{29} and Thr^{37} make multiple interfacial contacts in the PcTx1 : cASIC1 crystal structures, and some of these interactions were noted in our MD simulations (Table 1), yet there was no deleterious effect of mutating either residue to alanine. These residues appear to be further examples of interfacial residues that make intimate intermolecular contacts but do not contribute significantly to the strength of the protein–protein interaction (Bogan and Thorn, 1998).

Channel mutants were selected to assess the predictive power of the MD simulations rather than define the network of interacting residues on the channel. In agreement with the MD predictions, Asp^{349} (Asp^{350} in cASIC1) was previously shown to be important for PcTx1 inhibition of ASIC1a (Salinas *et al.*, 2006) and hence we did not mutate this residue. We selected Phe^{350} (Phe^{351} in cASIC1) as a positive control as it is known to be functionally important for the PcTx1 : ASIC1a interaction (Sherwood *et al.*, 2009), Glu^{235} as a negative control (no persistent contacts predicted by MD) and two intermediate cases (Tyr^{316} and Lys^{354}). Experiments with an F350A mutant confirmed the importance of Phe^{350} for PcTx1 activity (Sherwood *et al.*, 2009). These data, combined with our analysis of PcTx1 mutants in this study and previous work (Saez *et al.*, 2011), enable us to conclude that the intermolecular contacts observed in crystal structures of the PcTx1 : cASIC1 complex between Phe^{351} and PcTx1 residues Trp^{7} and Trp^{24} make crucial contributions to the strength of this bimolecular association.

Our channel mutagenesis data revealed an absence of critical intermolecular interactions involving residues Glu^{235}, Tyr^{316} and Lys^{354}. The Glu^{235} data confirmed predictions from the MD simulations. However, mutation of Tyr^{316} or Lys^{354} had no substantial effect on the ability of PcTx1 to alter channel activation or SSD, despite persistent interactions with PcTx1 in the MD simulations. This again highlights the point that just because two residues form close contacts at a protein–protein interface (e.g. based on structural data or MD simulations) does not necessarily mean that they contribute significantly to the free energy of binding as is commonly assumed.

A potential caveat of this study is that we used cASIC1 in MD simulations (because structures are not available for other species) but employed rASIC1a for functional studies. The latter is more relevant from a medicinal chemistry perspective as rASIC1a and hASIC1a are 97% identical and PcTx1 inhibits both channels by stabilizing the desensitized state. In contrast, PcTx1 induces activation of cASIC1, followed by slow decay to a steady-state current, thus stabilizing an open state (Baconguis and Gouaux, 2012). Despite this, the conformational differences between the PcTx1 binding site in the desensitized and open states of cASIC1 appears to be subtle (Baconguis and Gouaux, 2012; Gründer and Augustinowski, 2012). Thus, the cASIC1 structure used as a template for the MD studies should be a valid model. Indeed, the close agreement between our functional data on rASIC1a and MD simulations of the PcTx1 : cASIC1 complex supports the use of MD data to guide functional studies.

Conclusions

PcTx1 is a valuable lead molecule for development of therapeutically useful ASIC1a-selective inhibitors, and consequently, there is intense interest in understanding the molecular details of its interaction with ASIC1a. Although crystal structures of the PcTx1 : cASIC1 complex revealed an extensive network of >50 intermolecular contacts, we showed here that only ~50% of these interactions are essential for PcTx1 inhibition of rASIC1a. The identification of a binding hot spot on PcTx1 comprising residues Trp^{7}, Trp^{24}, Arg^{26}, Arg^{27}, Arg^{28} and Phe^{30} provides a crucial platform for design of small-molecule PcTx1 mimetics.

Acknowledgements

We acknowledge funding from the Australian National Health and Medical Research Council (Project Grant APP1012338 to G. F. K. and L. D. R., Principal Research Fellowship to G. F. K. and Early-Career Research Fellowship to E. D.), Australian Research Council (Future Fellowship to M. M.) and the Swiss National Science Foundation (Postdoctoral Fellowship to E. D.). We thank Prof. John Wood (University College London) for the rASIC1a clone. MD simulations were undertaken using resources provided by the NCI National Facility systems at the Australian National University as well as advanced computing resources provided by iVEC through the National Computational Merit Allocation Scheme supported by the Australian Government.

Author contributions

Conceived and analysed experiments: N. J. S., B. C.-A., I. C., L. D. R, M. M. and G. F. K. Performed experiments: N. J. S., B. C.-A., I. C., L. D. R., M. M. and J. L. Conceived, performed and analysed MD simulations: E. D. and A. E. M. All authors contributed to drafting the manuscript and read and approved the final version.

Conflict of interest

The authors declare no competing financial interest.

References

Alexander SP, Benson HE, Faccenda E, Pawson AJ, Sharman JL, Spedding M *et al.* (2013). The concise guide to pharmacology 2013/14: ligand-gated ion channels. Br J Pharmacol 170: 1582–1606.

Baconguis I, Gouaux E (2012). Structural plasticity and dynamic selectivity of acid-sensing ion channel-spider toxin complexes. Nature 489: 400–405.

Baron A, Schaefer L, Lingueglia E, Champigny G, Lazdunski M (2001). Zn^{2+} and H^+ are coactivators of acid-sensing ion channels. J Biol Chem 276: 35361–35367.

Berendsen HJC, Postma JPM, Van Gunsteren WF, Dinola A, Haak JR (1984). Molecular dynamics with coupling to an external bath. J Chem Phys 81: 3684–3690.

Berendsen HJC, Postma JPM, Van Gunsteren WF, Hermans J (1981). Interaction models for water in relation to protein hydration. In: Pullman B (ed). Intermolecular Forces. D. Riedel Publishing Company: Dordrecht, pp. 331–342.

Bogan AA, Thorn KS (1998). Anatomy of hot spots in protein interfaces. J Mol Biol 280: 1–9.

Chen X, Kalbacher H, Gründer S (2006). Interaction of acid-sensing ion channel (ASIC) 1 with the tarantula toxin psalmotoxin 1 is state dependent. J Gen Physiol 127: 267–276.

Chen X, Kalbacher H, Gründer S (2005). The tarantula toxin psalmotoxin 1 inhibits acid-sensing ion channel (ASIC) 1a by increasing its apparent H^+ affinity. J Gen Physiol 126: 71–79.

Chu XP, Xiong ZG (2013). Acid-sensing ion channels in pathological conditions. Adv Exp Med Biol 961: 419–431.

Coryell MW, Wunsch AM, Haenfler JM, Allen JE, Schnizler M, Ziemann AE *et al.* (2009). Acid-sensing ion channel-1a in the amygdala, a novel therapeutic target in depression-related behavior. J Neurosci 29: 5381–5388.

Dawson RJP, Benz J, Stohler P, Tetaz T, Joseph C, Huber S *et al.* (2012). Structure of the acid-sensing ion channel 1 in complex with the gating modifier psalmotoxin 1. Nat Comm 3: 936.

Deval E, Gasull X, Noel J, Salinas M, Baron A, Diochot S *et al.* (2010). Acid-sensing ion channels (ASICs): pharmacology and implication in pain. Pharmacol Ther 128: 549–558.

Durrant J, Mccammon JA (2011). Molecular dynamics simulations and drug discovery. BMC Biol 9: 71.

Dussor G (2015). ASICs as therapeutic targets for migraine. Neuropharmacology 94: 64–71.

Escoubas P, Bernard C, Lambeau G, Lazdunski M, Darbon H (2003). Recombinant production and solution structure of PcTx1, the specific peptide inhibitor of ASIC1a proton-gated cation channels. Prot Sci 12: 1332–1343.

Escoubas P, De Weille JR, Lecoq A, Diochot S, Waldmann R, Champigny G *et al.* (2000). Isolation of a tarantula toxin specific for a class of proton-gated Na^+ channels. J Biol Chem 275: 25116–25121.

Gründer S, Augustinowski K (2012). Toxin binding reveals two open state structures for one acid-sensing ion channel. Channels 6: 409–413.

Gründer S, Chen X (2010). Structure, function, and pharmacology of acid-sensing ion channels (ASICs): focus on ASIC1a. Int J Physiol Pathophysiol Pharmacol 2: 73–94.

Hesselager M, Timmermann DB, Ahring PK (2004). pH dependency and desensitization kinetics of heterologously expressed combinations of acid-sensing ion channel subunits. J Biol Chem 279: 11006–11015.

Hoagland EN, Sherwood TW, Lee KG, Walker CJ, Askwith CC (2010). Identification of a calcium permeable human acid-sensing ion channel 1 transcript variant. J Biol Chem 285: 41852–41862.

Israelachvili J, Pashley R (1982). The hydrophobic interaction is long range, decaying exponentially with distance. Nature 300: 341–342.

Izumi M, Ikeuchi M, Ji Q, Tani T (2012). Local ASIC3 modulates pain and disease progression in a rat model of osteoarthritis. J Biomed Sci 19: 77.

Jasti J, Furukawa H, Gonzales EB, Gouaux E (2007). Structure of acid-sensing ion channel 1 at 1.9 Å resolution and low pH. Nature 449: 316–323.

Jeffrey GA (1994). Hydrogen Bonding in Biological Structures. Springer-Verlag: Berlin.

Kellenberger S, Schild L (2002). Epithelial sodium channel/degenerin family of ion channels: a variety of functions for a shared structure. Physiol Rev 82: 735–767.

Kilkenny C, Browne W, Cuthill IC, Emerson M, Altman DG (2010). Animal research: Reporting *in vivo* experiments: the ARRIVE guidelines. Br J Pharmacol 160: 1577–1579.

Klint JK, Senff S, Saez NJ, Seshadri R, Lau HY, Bende NS *et al.* (2013). Production of recombinant disulfide-rich venom peptides for structural and functional analysis via expression in the periplasm of E. coli. PLoS One 8: e63865.

Klint JK, Smith JJ, Vetter I, Rupasinghe DB, Er SY (2015). Seven novel modulators of the analgesic target Nav1.7 uncovered using a high-throughput venom-based discovery pipeline. Br J Pharmacol 172: 2445–2458.

Kortemme T, Baker D (2002). A simple physical model for binding energy hot spots in protein–protein complexes. Proc Natl Acad Sci U S A 99: 14116–14121.

Kumar S, Nussinov R (2002). Close-range electrostatic interactions in proteins. Chembiochem 3: 604–617.

Li H, Robertson AD, Jensen JH (2005). Very fast empirical prediction and rationalization of protein pKa values. Proteins 61: 704–721.

Li WG, Xu TL (2015). Acid-sensing ion channels: a novel therapeutic target for pain and anxiety. Curr Pharm Des 21: 885–894.

McGrath J, Drummond G, McLachlan E, Kilkenny C, Wainwright C (2010). Guidelines for reporting experiments involving animals: the ARRIVE guidelines. Br J Pharmacol 160: 1573–1576.

Paukert M, Chen X, Polleichtner G, Schindelin H, Gründer S (2008). Candidate amino acids involved in H^+ gating of acid-sensing ion channel 1a. J Biol Chem 283: 572–581.

Pawson AJ, Sharman JL, Benson HE, Faccenda E, Alexander SP, Buneman OP *et al.* (2014). The IUPHAR/BPS Guide to PHARMACOLOGY: an expert-driven knowledgebase of drug targets and their ligands. Nucl Acids Res 42 (Database Issue): D1098–106.

Qi D, Scholthof KB (2008). A one-step PCR-based method for rapid and efficient site-directed fragment deletion, insertion, and substitution mutagenesis. J Virol Methods 149: 85–90.

Ramaswamy SS, Maclean DM, Gorfe AA, Jayaraman V (2013). Proton-mediated conformational changes in an acid-sensing ion channel. J Biol Chem 288: 35896–35903.

Saez NJ, Mobli M, Bieri M, Chassagnon IR, Malde AK, Gamsjaeger R *et al.* (2011). A dynamic pharmacophore drives the interaction between psalmotoxin-1 and the putative drug target acid-sensing ion channel 1a. Mol Pharmacol 80: 796–808.

Salinas M, Rash LD, Baron A, Lambeau G, Escoubas P, Lazdunski M (2006). The receptor site of the spider toxin PcTx1 on the proton-gated cation channel ASIC1a. J Physiol 570: 339–354.

Samways DS, Harkins AB, Egan TM (2009). Native and recombinant ASIC1a receptors conduct negligible Ca^{2+} entry. Cell Calcium 45: 319–325.

Schmid N, Eichenberger AP, Choutko A, Riniker S, Winger M, Mark AE *et al.* (2011). Definition and testing of the GROMOS force-field versions 54A7 and 54B7. Eur Biophys J 40: 843–856.

Sherwood T, Franke R, Conneely S, Joyner J, Arumugan P, Askwith C (2009). Identification of protein domains that control proton and calcium sensitivity of ASIC1a. J Biol Chem 284: 27899–27907.

Sherwood TW, Lee KG, Gormley MG, Askwith CC (2011). Heteromeric acid-sensing ion channels (ASICs) composed of ASIC2b and ASIC1a display novel channel properties and contribute to acidosis-induced neuronal death. J Neurosci 31: 9723–9734.

Stone AJ (1996). The Theory of Intermolecular Forces. Clarendon Press: Oxford.

Van Der Spoel D, Lindahl E, Hess B, Groenhof G, Mark AE, Berendsen HJC (2005). GROMACS: fast, flexible, and free. J Comp Chem 26: 1701–1718.

Waldmann R, Champigny G, Bassilana F, Heurteaux C, Lazdunski M (1997). A proton-gated cation channel involved in acid-sensing. Nature 386: 173–177.

Wemmie JA, Taugher RJ, Kreple CJ (2013). Acid-sensing ion channels in pain and disease. Nat Rev Neurosci 14: 461–471.

Xiong Z-G, Zhu X-M, Chu X-P, Minami M, Hey J, Wei W-L *et al.* (2004). Neuroprotection in ischemia: blocking calcium-permeable acid-sensing ion channels. Cell 118: 687–698.

Ziemann AE, Schnizler MK, Albert GW, Severson MA, Howard MA 3rd, Welsh MJ *et al.* (2008). Seizure termination by acidosis depends on ASIC1a. Nat Neurosci 11: 816–822.

Supporting Information

Additional Supporting Information may be found in the online version of this article at the publisher's web-site:

http://dx.doi.org/10.1111/bph.13267

Figure S1 Fully assigned 2D 1H-15N HSQC spectrum of wild-type PcTx1 (black) overlaid on HSQC spectra of the mutants K6A (magenta) and W7A (teal) acquired under identical conditions.

Figure S2 Fully assigned 2D 1H-15N HSQC spectra of wild-type PcTx1 (black) overlaid on a HSQC spectrum of the V32A mutant (red) acquired under identical conditions. Peaks from the backbone amide groups of Asn12 and Glu31 are not visible in this spectrum.

Figure S3 pH-dependence of steady-state desensitisation (blue squares) and activation (black circles) for WT rASIC1a (**A**) and the rASIC1a mutants E235A (**B**), Y316A (**C**), F350A (**D**), and K354A (**E**). Curves are shown in the absence (solid symbols and lines) and presence of 30 nM PcTx1 (open symbols, dashed lines). Residue numbering is given for both rASIC1a and cASIC1 (in parentheses). Data points are mean ± SEM ($n = 4–8$). The inhibitory efficiency of 30 nM PcTx1 applied 0.10–0.15 pH units higher than the pH_{50} of SSD is given in red in each panel.

Figure S4 Normalised histogram of the fractional occurrences for (**A**) hydrogen bonds and (**B**) other non-bonded interactions calculated from MD simulations of the PcTx1:cASIC1 complex. For each peptide-channel contact found in the co-crystal structure (PDB 3S3X) the fractional occurrence was calculated by counting the number of frames from the simulations in which the contact was within a given cut-off. Cut-offs of 2.5 Å and 5 Å were used for hydrogen bonds and non-bonded interactions, respectively. Fractional occurrences were averaged over the three peptides in the simulation system and over the three independent simulation trajectories. The fractional occurrences of all contacts were binned to obtain the normalised histogram.

Table S1 Mean pH_{50} values of activation and steady-state desensitisation curves for WT and mutant rASIC1a channels, both in the presence and absence of PcTx1. Data are mean ± SEM ($n = 4–8$). *, $p < 0.05$ (difference in pH_{50} of mutant channels compared to WT rASIC1a).